


## Article

# Preparation and Characterization of Bilayer Polymer-Dispersed Liquid Crystals Doped with Gd<sub>2</sub>O<sub>3</sub> Nanoparticles and Rhodamine B Base Fluorescent Dye

Yongle Wu <sup>1,2,†</sup>, Yuzhen Zhao <sup>1,†</sup>, Xun Li <sup>1</sup>, Hong Gao <sup>3</sup>, Zhun Guo <sup>1</sup>, Dong Wang <sup>2,\*</sup> , Yi Luan <sup>2</sup>  and Lei Wang <sup>4</sup> 

<sup>1</sup> Xi'an Key Laboratory of Advanced Photo-Electronics Materials and Energy Conversion Device, School of Electronic Information, Xijing University, Xi'an 710123, China; wuyongle1999@163.com (Y.W.); zyz19870226@163.com (Y.Z.); lixun1999814@163.com (X.L.); guozhun@xijing.edu.cn (Z.G.)

<sup>2</sup> Department of Materials Physics and Chemistry, School of Materials Science and Engineering, University of Science and Technology Beijing, Beijing 100083, China; yiluan@ustb.edu.cn

<sup>3</sup> Division of Material Engineering, China Academy of Space Technology, Beijing 100094, China; gaohong\_cast@sina.com

<sup>4</sup> Key Laboratory of Chemical Additives for China National Light Industry, Shaanxi Key Laboratory of Chemical Additives for Industry, College of Chemistry & Chemical Engineering, Shaanxi University of Science & Technology, Xi'an 710021, China; wanglei@sust.edu.cn

\* Correspondence: wangdong@ustb.edu.cn

† These authors contributed equally to this work.

**Abstract:** Using the polymerization-induced phase separation (PIPS) method, bilayer polymer-dispersed liquid crystal (PDLC) films with a PDLC-PVA-PDLC structure were prepared in this work. It was found that all PDLC performance indexes were affected by polymer mesh size after comparing the microscopic morphology and electro-optical properties of samples with different monomer ratios. Gd<sub>2</sub>O<sub>3</sub> nanoparticles and rhodamine B base fluorescent dyes introduced into the bilayer PDLC optimized the samples' electro-optical properties and developed new functionalities. In addition, the bilayer PDLC doped with Gd<sub>2</sub>O<sub>3</sub> and rhodamine B base held excellent progressive driving functions as well as stable durability properties. Samples doped with Gd<sub>2</sub>O<sub>3</sub> nanoparticles and rhodamine B base also produced excellent anti-counterfeiting effects under UV irradiation at different angles, further exploiting the application potential of PDLC.

**Keywords:** polymer-dispersed liquid crystal; bilayer; electro-optical properties; Gd<sub>2</sub>O<sub>3</sub> nanoparticles; fluorescent dyes



**Citation:** Wu, Y.; Zhao, Y.; Li, X.; Gao, H.; Guo, Z.; Wang, D.; Luan, Y.; Wang, L. Preparation and Characterization of Bilayer Polymer-Dispersed Liquid Crystals Doped with Gd<sub>2</sub>O<sub>3</sub> Nanoparticles and Rhodamine B Base Fluorescent Dye. *Molecules* **2024**, *29*, 1126. <https://doi.org/10.3390/molecules29051126>

Academic Editors: Ana Catarina Trindade, João Canejo and Pedro De Almeida

Received: 1 February 2024

Revised: 23 February 2024

Accepted: 29 February 2024

Published: 2 March 2024



**Copyright:** © 2024 by the authors. Licensee MDPI, Basel, Switzerland. This article is an open access article distributed under the terms and conditions of the Creative Commons Attribution (CC BY) license (<https://creativecommons.org/licenses/by/4.0/>).

## 1. Introduction

As a typical liquid crystal-based optical film, polymer-dispersed liquid crystal (PDLC) consists of a polymer substrate with embedded micrometer- or nanometer-sized liquid crystal (LC) microdroplets [1]. PDLC films exhibit an opaque state under unelectrified conditions due to the random orientation of LC microdroplets [2]. In turn, when a sufficiently large voltage is applied, LC microdroplets align themselves along the direction of the electric field and cause PDLCs to reach a transparent state with high transmittance [3]. Based on the above features, PDLC has been widely used in smart windows [4–6], displays [7,8], and optical switches [9–11]. Furthermore, PDLC is favored in low energy-consuming buildings [12–14], semiconductors [15], field-effect transistors [16], and solar concentrators [17].

In previous studies, functionalization and performance optimization of PDLC were achieved by optimizing polymerization conditions, adjusting precursor ratios [18,19], and doping with additional [17] special properties. Deng et al. [20] designed and prepared an ultrafast, switchable, and passive radiative cooling smart window based on PDLC that exhibited enhanced infrared emissivity in the 8–13 μm wavelength range. The novel

PDLC/GO nanocomposite designed by Cheng et al. [21] responded to NIR-Vis-UV light and could be applied to soft actuators and optomechanical systems driven directly by sunlight. PDLCs accomplish fast switching speeds, large optical modulation, and robust mechanical stability using silver nanowire micromesh as electrodes, as demonstrated by Zhang et al. [22]. Shivaraja et al. [23] found that doping octadecylamine functionalized single-walled carbon nanotubes (ODA-SWCNTs) in PDLC could reduce threshold voltage and response time. The photoinitiator concentration directly affected the phase separation process, which determined the morphology and electro-optical properties of PDLCs, according to Nasir et al. [24]. In addition, other fluorescent dyes and inorganic nanoparticles were doped into PDLC for modification. Reticular nanofiber films containing the fluorescent material ST18 were blended into PDLC and improved electro-optical and fluorescent properties, according to Shi et al. [25]. Electro-optical properties were enhanced by doping SiO<sub>2</sub> nanoparticles into PDLC by Kim et al. [26]. Katariya-Jain et al. found that carbon nanoparticle doping could enhance thermo-electro-optical and dielectric properties in PDLC [27].

To compensate for the shortcomings of monolayer materials, multilayer [28,29] structures have become a research hotspot with applications to a variety of fields in recent years. Using a layer-by-layer method, Khoi et al. [30] deposited a polymer multi-layer membrane consisting of poly allylamine hydrochloride and poly styrene sulfonate on the cation-exchange membrane, which achieved selective recovery of Na ions. Multilayer films prepared by Culebras et al. [31] had high conductivity and Seebeck coefficients with alternately depositing layers of aqueous solutions of PEDOT: NPs and double-walled carbon nanotubes (DWNT) stabilized with PEDOT: PSS via a layer-by-layer methodology. The multilayer composite electrolyte designed and prepared by Park et al. [32] displayed excellent cyclic stability for application in lithium–sulfur batteries. The multilayer structure consisting of paper, TPS and PLA, PBAT, PHBV, or PVOH by Eslami et al. [33] not only improved the dry and wet strength of the paper but also showed considerable resistance to oil and grease. Low dielectric properties of monolayer in-plane heterostructures prevent the generation of high concentrations of thermally excited carriers from doped impurities. Ogura et al. [34] solved this problem by developing multilayer in-plane heterostructures.

However, conventional monolayer PDLC suffers from certain drawbacks, such as difficulty accessing the intermediate state between the on-state and off-state. It greatly limits the further development of PDLC. In this study, bilayer PDLC films were prepared by introducing the concept of multilayer structures into PDLC, which can access the intermediate state and achieve progressive driving functions. In addition, Gd<sub>2</sub>O<sub>3</sub> nanoparticles and fluorescent dyes were doped into the bilayer PDLC to further improve its electro-optical properties and confer functionalization. The stable PDLC–PVA–PDLC structure also enables the bilayer PDLC to perform well in durability tests, and a longer service life can meet liquid crystal optical film application requirements.

## 2. Experimental

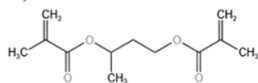
### 2.1. Materials

SLC1717 ( $n_o = 1.519$ ,  $n_e = 1.720$ ,  $\Delta n = 0.201$ ,  $T_c = 92\text{ }^\circ\text{C}$ ), the nematic phase liquid crystal used in this experiment, was purchased from Shijiazhuang Chengzhi Yonghua Display Materials Co. (Shijiazhuang, China). As a mixture of UV polymerizable monomers, UV6301 was bought from Kuer Industries (Shanghai) Co. (Shanghai, China). As a cross-linker and fluorescent dye, 1,4 Butanediol dimethacrylate (BDDMA) and Rhodamine B base were purchased from Beijing Bailingwei Technology Co. (Beijing, China), respectively. The free radical photoinitiator 2,2-dimethoxy-2-phenylacetophenone (IRG651) was purchased from Anhui Zesheng Technology Co. (Anqing, China).

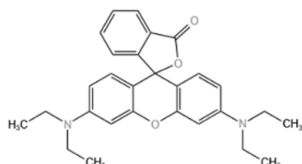
Gd<sub>2</sub>O<sub>3</sub> nanoparticles (diameter 40–60 nm), the inorganic nanoparticles used in this experiment, were acquired from Alab (Shanghai, China) Chemical Technology Co. (Shanghai, China). Oleic acid, a modifier for the nanoparticles, was bought from Sinopharm Chemical Reagent Co. (Shanghai, China). The specific chemical structures of materials used in this study

are presented in Figure 1. The  $\text{Gd}_2\text{O}_3$  nanoparticles were surface-modified using oleic acid to inhibit their agglomeration and uniformly disperse them in the LC/monomer mixtures.

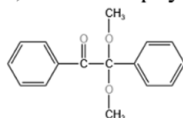
(a) 1,4-Butanediol dimethacrylate: BDDMA



(b) Rhodamine B base



(c) 2,2-Dimethoxy-2-phenylacetophenone: IRG651



(d) Oleic acid

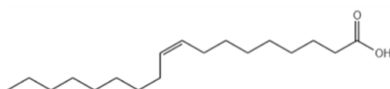


**Figure 1.** The specific chemical structure of the materials used.

Details concerning the surface modification treatment of  $\text{Gd}_2\text{O}_3$  nanoparticles are described as follows. The  $\text{Gd}_2\text{O}_3$  nanoparticles (10 mmol) were scattered in tetrahydrofuran (20 mL) and mechanically stirred (300–600 rpm) at 65 °C for 30 min for homogeneous mixing. The oleic acid (5 mL)/tetrahydrofuran (10 mL) mixture was poured into the  $\text{Gd}_2\text{O}_3$  solution and continuously stirred for 30 min under heating conditions. Oleic acid (2 mL) was mixed into the  $\text{Gd}_2\text{O}_3$  solution for 5 min and the procedure was repeated five times. For adequate modification, the above mixture was mechanically stirred (300–600 rpm) at 85 °C for 2 h. The heating process described above must be conducted under condensing conditions to avoid tetrahydrofuran volatilization. Afterward, the heat source was removed to cool the mixture to room temperature. The precipitate was obtained after centrifuging (5000 rpm, 5 min), separating the above blend, and washing five times with anhydrous ethanol for primary modified  $\text{Gd}_2\text{O}_3$  nanoparticles. The above primary modified  $\text{Gd}_2\text{O}_3$  nanoparticles were solubilized in the oleic acid (5 mL)/hexane (20 mL) mixture and mechanically stirred (800~1000 rpm) for 2 h. The precipitate was obtained after centrifuging (5000 rpm, 10 min), separating the above blend, washing five times with anhydrous ethanol, and then drying to obtain secondary modified  $\text{Gd}_2\text{O}_3$  nanoparticles.

## 2.2. Sample Preparation

PVA films are ideal for preparing bilayer PDLC interlayers due to their excellent mechanical properties. In addition, PVA film is immiscible with LC, which is critical for preparing bilayer PDLC. The procedures for specific preparation are as follows.

1. Preparing precursors: LC/monomer/initiator blends in different proportions were shaken for 3 min, stirred for 5 min, and sonicated for 15 min to produce a uniform phase. Specific percentages are described in Tables 1–3;
2. Preparing monolayer PDLC: LC cells were prepared using an 8  $\mu\text{m}$  thick polyimide film as a spacer to hold two single-sided conductive glass substrates apart. Mixtures a1~a6 in Table 1 were injected into LC cells by capillary action, and monolayer PDLC samples were obtained after polymerization. The polymerization time, light intensity, and temperature for this set of samples were 6 min, 4.5 mW/cm<sup>2</sup>, and 35 °C, respectively;

3. Preparing PVA films: A layer of aqueous PVA solution (0.05 wt%) was placed on the glass substrate with surface treatment using surface tension. Glass substrates with PVA films adhered to the surface were obtained by storing them at a temperature of 75 °C for 3 h;
4. Preparing bilayer PDLC: The ratios of various substances in the upper and lower layers of the bilayer PDLC are shown in Tables 2 and 3, respectively. An 8 µm thick polyimide film was used to separate the glass substrate with PVA film on the surface from the unilateral conductive glass substrate and fixed to obtain the LC cell. The upper PDLC precursor was injected into the LC cell by capillary action, and PDLC-PVA composite films were obtained after curing. The glass substrates with PDLC-PVA composite film on the surface were obtained by peeling off the surface-treated glass substrates. The glass substrates attached with PDLC-PVA composite film on the surface were separated from the one-sided conductive glass substrates using 8 µm thick polyimide films to obtain new LC cells. The lower PDLC precursors were injected into new LC cells by capillary action, and bilayer PDLC films with a PDLC-PVA-PDLC structure were acquired after polymerization.

**Table 1.** The composition of Group A <sup>a</sup>.

Sample	Weight Percentage (wt%)		
	SLC1717	UV6301	BDDMA
Group A			
a1	50	50	0
a2	50	49	1
a3	50	48	2
a4	50	47	3
a5	50	46	4
a6	50	45	5

<sup>a</sup> The weight of the photo-initiator IRG651 is 0.5% of the total weight.

**Table 2.** The upper compositions of Groups B and C.

Sample	Weight Percentage (wt%)				
	SLC1717	UV6301	BDDMA	Gd <sub>2</sub> O <sub>3</sub> Nanoparticles	Rhodamine B Base
Group B					
b1	50	49	1	0.0	0.0
b2	50	49	1	0.2	0.0
b3	50	49	1	0.4	0.0
b4	50	49	1	0.6	0.0
b4	50	49	1	0.8	0.0
b6	50	49	1	1.0	0.0
Group C					
c1	50	49	1	0.2	0.0
c2	50	49	1	0.2	0.2
c3	50	49	1	0.2	0.4
c4	50	49	1	0.2	0.6
c5	50	49	1	0.2	0.8
c6	50	49	1	0.2	1.0

Among them, the variables of Groups B and C were the Gd<sub>2</sub>O<sub>3</sub> nanoparticle and Rhodamine B base content, respectively, as shown in Tables 2 and 3.



**Table 3.** The lower composition of Groups B and C.

Sample	Weight Percentage (wt%)				
	SLC1717	UV6301	BDDMA	Gd <sub>2</sub> O <sub>3</sub> Nanoparticles	Rhodamine B Base
Group B					
b1	50	47	3	0.0	0.0
b2	50	47	3	0.2	0.0
b3	50	47	3	0.4	0.0
b4	50	47	3	0.6	0.0
b4	50	47	3	0.8	0.0
b6	50	47	3	1.0	0.0
Group C					
c1	50	47	3	0.2	0.0
c2	50	47	3	0.2	0.2
c3	50	47	3	0.2	0.4
c4	50	47	3	0.2	0.6
c5	50	47	3	0.2	0.8
c6	50	47	3	0.2	1.0

### 2.3. Characterization

To verify whether oleic acid was attached to the surface of Gd<sub>2</sub>O<sub>3</sub> nanoparticles, its chemical composition was characterized using Fourier-Transform Infrared Spectrometry (FTIR, INVENIO S, Bruker Optics GmbH & Co. KG, Ettlingen, Germany).

Electro-optical characteristics are one of the most critical metrics and can usually measure the application potential of PDLC. In this experiment, the electro-optical curve, response time curve, and contrast ratio were evaluated with the Liquid Crystal Comprehensive Parameter Tester (LCT-5016C, Beijing LCD Engineering Research and Development Center, Beijing, China). Additionally, other vital variables such as threshold voltage ( $V_{th}$ ), saturation voltage ( $V_{sat}$ ), off-state transmittance ( $T_{off}$ ), and off-state response time ( $t_{off}$ ) were also obtained from electro-optical characterization tests. Herein,  $V_{th}$  and  $V_{sat}$  were attained once the transmittance of the bilayer PDLC reached 10% and 90% of its maximum value, respectively. The ratio of on-state to off-state transmittance is called the contrast ratio (CR).

The polymer matrix morphology was observed by scanning electron microscopy (SEM, ZEISS SUPRA55, Carl Zeiss AG, Oberkochen, Germany). Samples were pretreated prior to observation as follows: PDLC samples were immersed in cyclohexane for 15 d at room temperature to clear all LC molecules. The cyclohexane was renewed every three days during the soaking process to ensure the adequate deletion of LC molecules. After soaking, the samples were dried at 60 °C for 1 h to remove residual cyclohexane from the surface. After drying, the samples were sprayed with gold under a vacuum for SEM visualization.

The fluorescence emission spectra of bilayer PDLC samples doped with Rhodamine B base were characterized using a steady-state transient fluorescence spectrometer (Edinburgh Instruments, Livingston, UK, FLS 1000), and fluorescence emission curves were obtained for different doping concentrations.

The samples were tested for transmittance at different wavelengths with the Lambda 950 UV/VIS/NIR spectrophotometer (Perkin-Elmer, Waltham, MA, USA) at room temperature and transmittance–wavelength curves were obtained for the bilayer PDLC at different voltages.

## 3. Results and Discussions

### 3.1. Effect of the Crosslinker Content on the Property of Monolayer PDLC

Crosslinking agents connect polymer chains and reduce the size of the polymer mesh. The SEM image of the polymer mesh with variations in crosslinker BDDMA content is shown in Figure 2. As the crosslinker content increased, the number of crosslinking points in the polymer network also increased, leading to a decrease in the size of the polymer mesh.

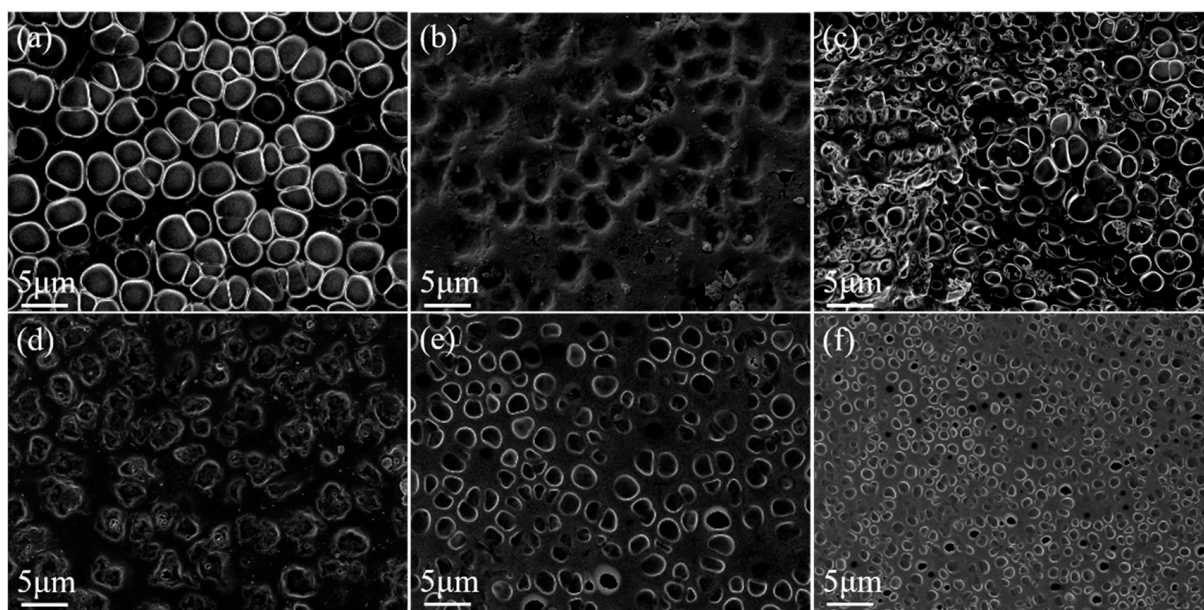


**Figure 2.** SEM images of PDLC cells. (a) 0 wt% BDDMA; (b) 1 wt% BDDMA; (c) 2 wt% BDDMA; (d) 3 wt% BDDMA; (e) 4 wt% BDDMA; (f) 5 wt% BDDMA. 3000 $\times$  magnification.

Variations in polymer micromorphology led to changes in the electro-optical properties of PDLC, as depicted in Figure 3. The anchoring force on LC droplets increases with smaller polymer meshes, which shifts the transmittance-voltage curve to the right and raises  $V_{th}$  and  $V_{sat}$ , as demonstrated in Figure 3a,b.  $V_{th}$  and  $V_{sat}$  were enlarged from 5.3 V and 10.0 V to 26.4 V and 66.9 V, respectively, when BDDMA content increased from 0 to 5 wt%. The growth of  $V_{sat}$  was greater than  $V_{th}$ , increasing  $\Delta V$  from 4.7 V to 40.5 V. Changes in polymer morphology can cause variation in the refractive index match between the polymer and LC microdroplets, altering the  $T_{off}$  and CR of the PDLC, as illustrated in Figure 3c. The refractive index match between the polymer and the LC microdroplets was weakened with increasing BDDMA content, causing a gradual decrease in  $T_{off}$  from 13.6% to 4.2%. CR gradually grew from 7.3 to 23.8 as the CR tendency became contrary to  $T_{off}$ . The larger the anchoring force, the simpler it is for the LC microdroplets to recover from an ordered state to a disordered state. The  $t_{off}$  decreased from 78.8 ms to 7.1 ms as depicted in Figure 3d.

### 3.2. $Gd_2O_3$ Nanoparticles Doped Bilayer PDLC

#### 3.2.1. Modification of $Gd_2O_3$ Nanoparticles

$Gd_2O_3$  nanoparticles were modified with oleic acid to prevent agglomeration and promote uniform dispersion in the precursors of LC/UV polymerizable monomers. The FTIR spectra of  $Gd_2O_3$  nanoparticles before and after modification are shown in Figure 4. Compared to pre-modification, the modified  $Gd_2O_3$  nanoparticles showed a characteristic peak at 2900  $cm^{-1}$ , which represents the stretching vibration peak of the methylene group. It can be seen that oleic acid was successfully modified on the surface of  $Gd_2O_3$  nanoparticles.

#### 3.2.2. Effect of $Gd_2O_3$ Nanoparticle Content on the Properties of Bilayer PDLC

$Gd_2O_3$  nanoparticles affect polymers' microscopic morphology, as indicated in Figures 5 and 6.  $Gd_2O_3$  nanoparticles could access LC microdroplets and increase their size, thus changing the polymer's micromorphology. As  $Gd_2O_3$  nanoparticle content increased, the size of LC microdroplets also increased, resulting in a gradual increase in polymer mesh size.

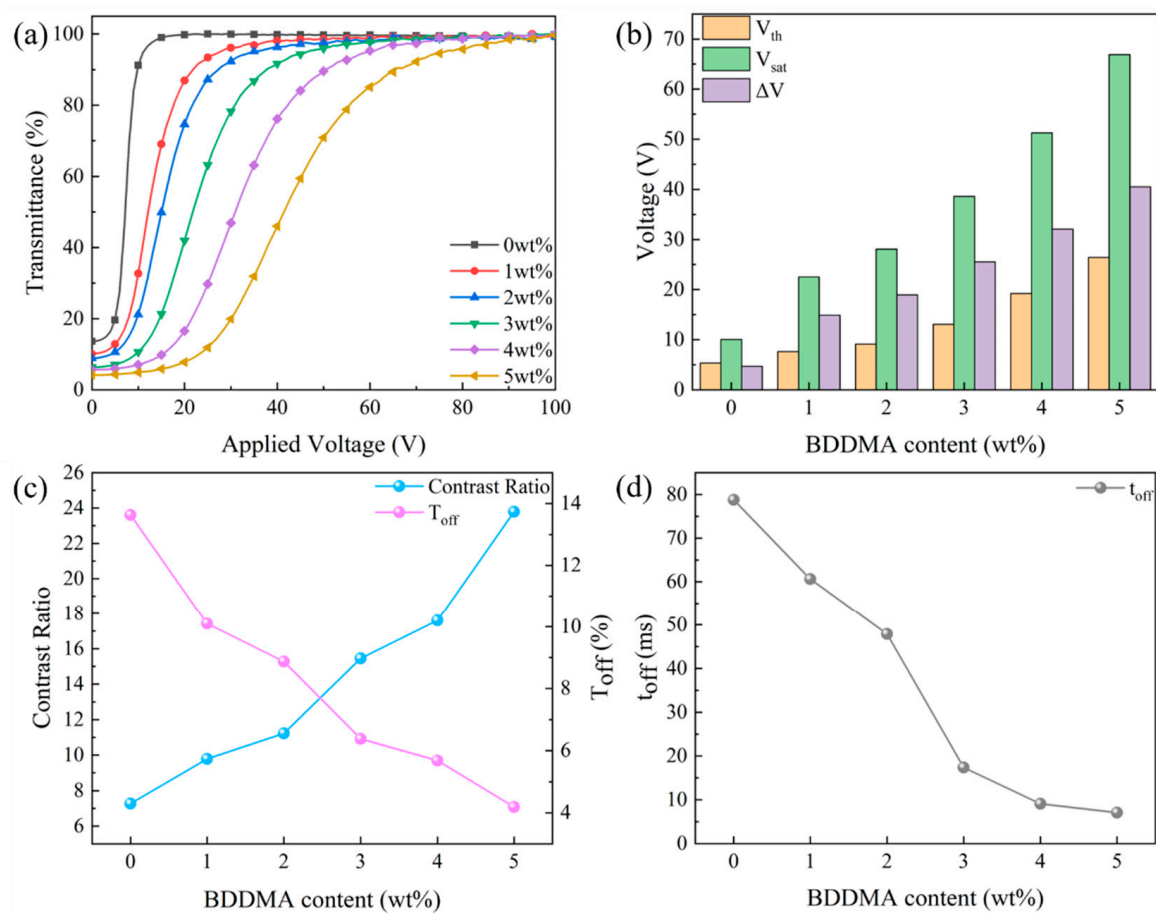


**Figure 3.** The effect of cross-linker (BDDMA) content on electro-optical properties: (a) voltage-transmittance curve; (b) threshold voltage ( $V_{th}$ ), saturation voltage ( $V_{sat}$ ), and  $\Delta V$ ; (c) contrast ratio (CR) and off-state transmittance ( $T_{off}$ ); (d) response time ( $t_{off}$ ).

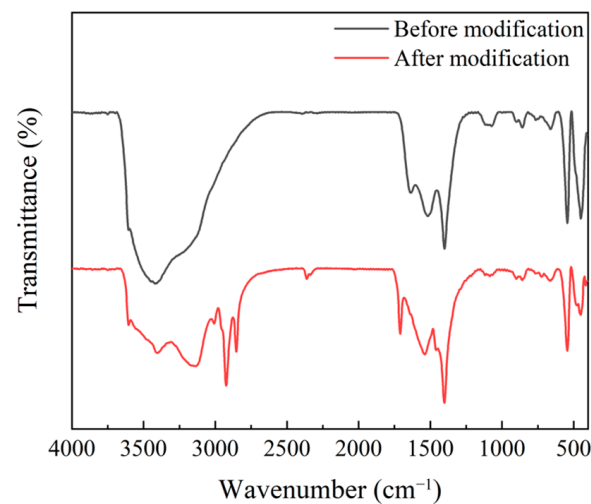


**Figure 4.** Fourier-transform infrared (FTIR) spectra of  $Gd_2O_3$  nanoparticles before and after modification.



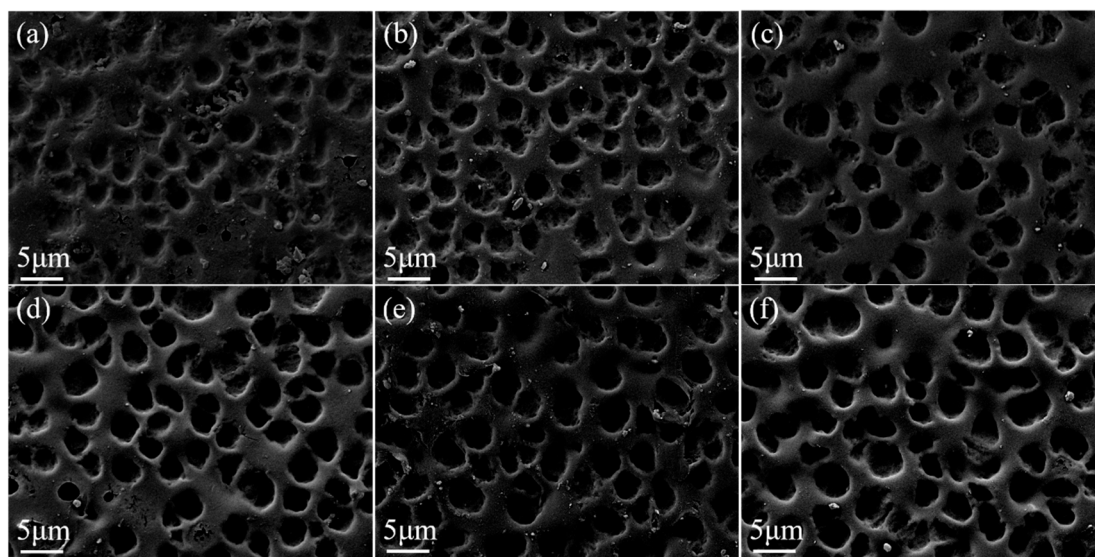


**Figure 5.** SEM images of upper-layer PDLC cells. (a) 0.0 wt%; (b) 0.2 wt%; (c) 0.4 wt%; (d) 0.6 wt%; (e) 0.8 wt%; (f) 1.0 wt%  $\text{Gd}_2\text{O}_3$  nanoparticles doped. 3000 $\times$  magnification.

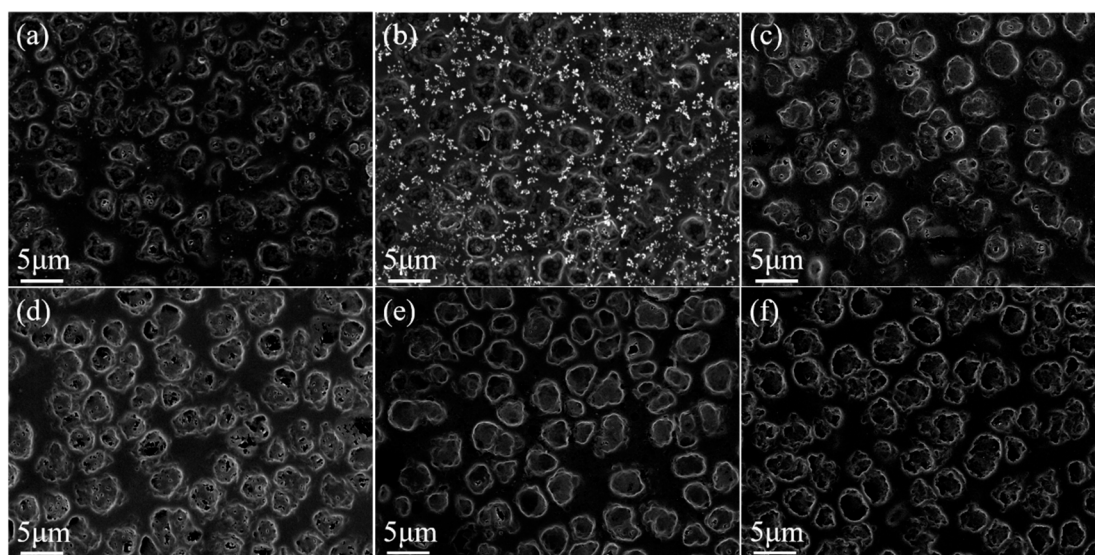


**Figure 6.** SEM images of lower-layer PDLC cells. (a) 0.0 wt%; (b) 0.2 wt%; (c) 0.4 wt%; (d) 0.6 wt%; (e) 0.8 wt%; (f) 1.0 wt%  $\text{Gd}_2\text{O}_3$  nanoparticles doped; 3000 $\times$  magnification.

As shown in Figure 7, the fraction of  $\text{Gd}_2\text{O}_3$  nanoparticles significantly impacts the electro-optical properties of the bilayer PDLC. Electro-optical curves migrated to the right and then left as the size of the polymer mesh increased in Figure 7a. While the percentage of  $\text{Gd}_2\text{O}_3$  nanoparticles enlarged from 0 to 0.4 wt%, the anchoring force applied to the LC droplets progressively declined, bringing about reductions in  $V_{\text{th}}$  and  $V_{\text{sat}}$  of the bilayer PDLC from 30.2 V and 79.8 V to 17.8 V and 50.4 V, respectively. Since the reduced value of  $V_{\text{sat}}$  was greater than  $V_{\text{th}}$ ,  $\Delta V$  decreased, according to Figure 7b. With the increase in  $\text{Gd}_2\text{O}_3$  nanoparticles to 1 wt%,  $V_{\text{th}}$  and  $V_{\text{sat}}$  gradually increased to 36.2 V and 83.9 V, while  $\Delta V$  was roughly kept at 50 V.

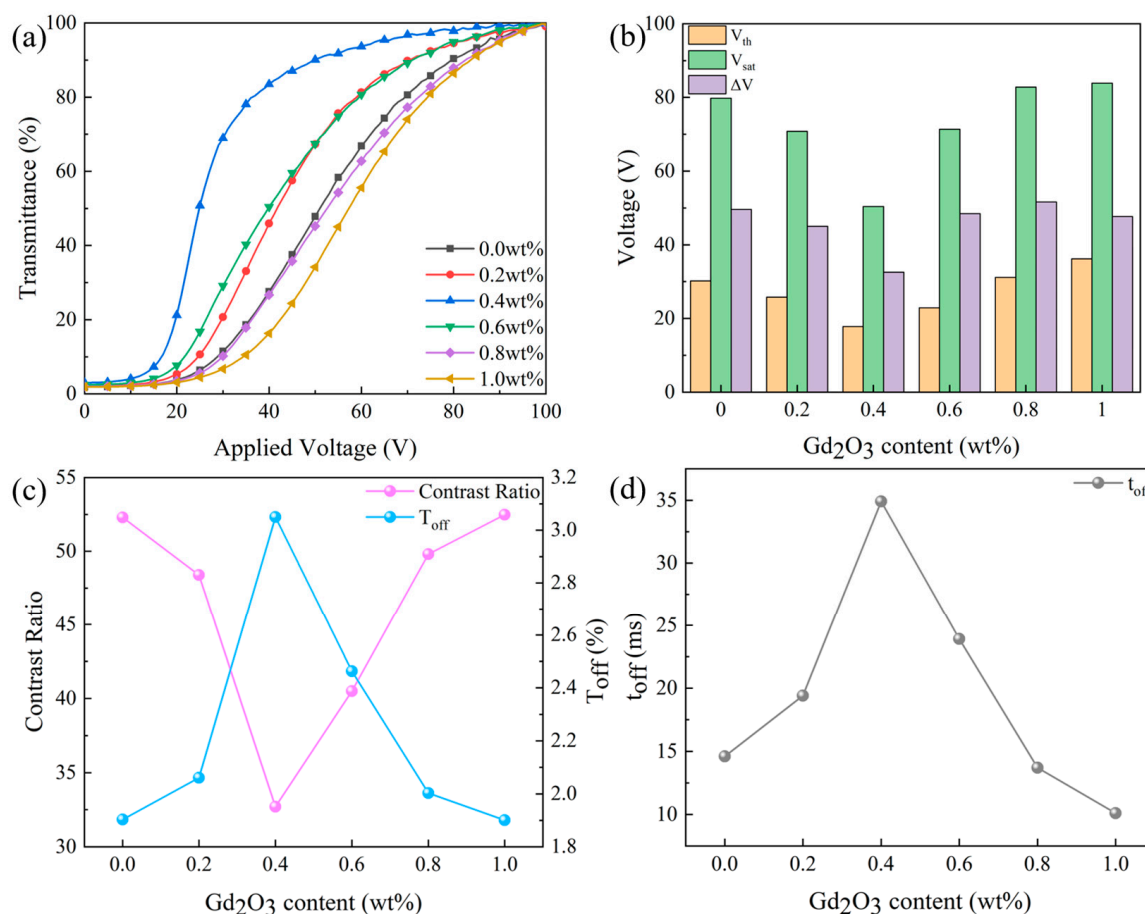


**Figure 7.** The effect of  $\text{Gd}_2\text{O}_3$  nanoparticle content on electro-optical properties. (a) voltage-transmittance curve; (b) threshold voltage ( $V_{th}$ ), saturation voltage ( $V_{sat}$ ), and  $\Delta V$ ; (c) contrast ratio (CR) and off-state transmittance ( $T_{off}$ ); (d) response time ( $t_{off}$ ).

Additionally, the fraction of  $\text{Gd}_2\text{O}_3$  nanoparticles impacted the  $T_{off}$  and CR of bilayer PDLC, as demonstrated in Figure 7c. The increase in  $\text{Gd}_2\text{O}_3$  nanoparticle content from 0 to 0.4 wt% improved the  $T_{off}$  from 1.9% to 3.0%. However, a further increase in  $\text{Gd}_2\text{O}_3$  nanoparticle content to 1.0 wt% brought about a decrease in  $T_{off}$  to 1.9%. Given that the CR's tendency was the opposite of  $T_{off}$ , the CR first decreased from 52.3 to 32.71 and then increased to 52.5. Variations in  $\text{Gd}_2\text{O}_3$  nanoparticle content affected the time required for LC droplets to transition from an ordered to a disordered state, as observed in Figure 7d. By increasing the  $\text{Gd}_2\text{O}_3$  nanoparticle content from 0 to 0.4 wt%, the  $t_{off}$  increased from 14.6 ms to 34.9 ms. However, as the nanoparticle content was further extended to 1.0 wt%, the  $t_{off}$  decreased to 10.1 ms.

The EDS map of the sample with the optimal  $\text{Gd}_2\text{O}_3$  nanoparticle content (b2) is shown in Figure 8. According to the Gd elemental distribution, the  $\text{Gd}_2\text{O}_3$  nanoparticles are more uniformly distributed. In addition, the agglomeration of  $\text{Gd}_2\text{O}_3$  nanoparticles is not obvious, which is a prerequisite for maintaining PDLC's excellent performance.

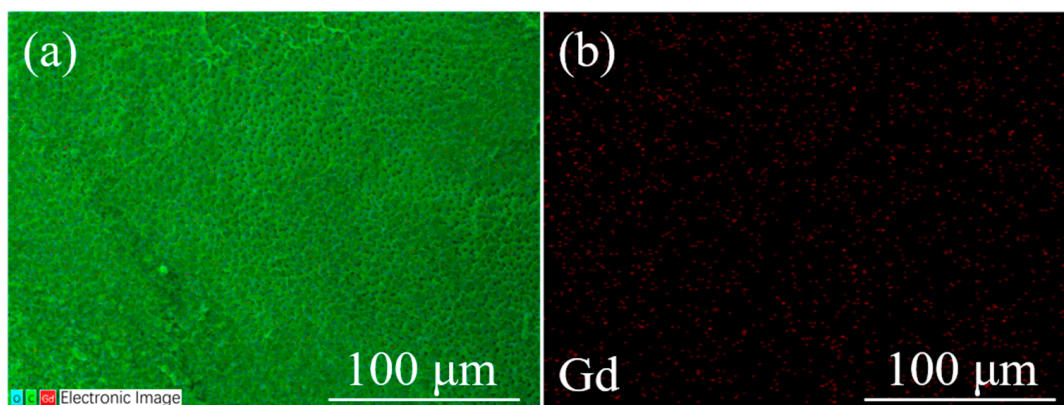


**Figure 8.** EDS mapping of the optimal sample (b2). (a) The distribution of all elements and (b) the distribution of Gd elements.

### 3.2.3. Progressive Driving Test of Bilayer PDLC Doped with $\text{Gd}_2\text{O}_3$ Nanoparticles

The change in transmittance was observed by applying different voltages to the sample and verifying the progressive driving performance of the bilayer PDLC. As the applied voltage increased, there was a stepwise growth in the sample transmittance, as shown in the physical diagram in Figure 9. The reason for this result is that the two monolayer PDLC samples have different drive voltages so both cannot be driven simultaneously. The cross-sectional SEM image of the bilayer PDLC is plotted in Figure 10, where one layer of the PDLC is easier to drive and the other is more difficult to drive.

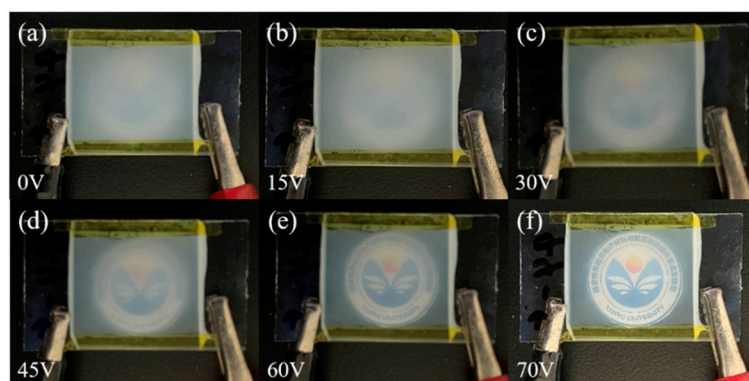


**Figure 9.** Physical plots of transmittance variation for the optimum sample at different voltages: (a) 0 V, (b) 15 V, (c) 30 V, (d) 45 V, (e) 60 V, and (f) 70 V, respectively.

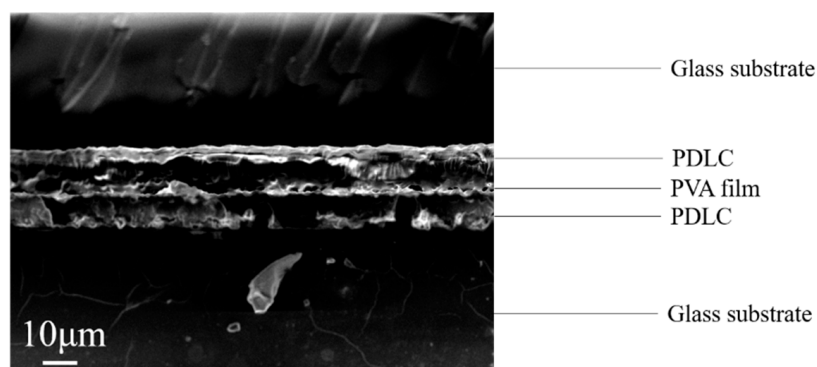


**Figure 10.** SEM image of a bilayer PDLC cross-section with a PDLC–PVA–PDLC structure.



### 3.3. Fluorescent Dye Rhodamine B Base Doped Bilayer PDLC

#### 3.3.1. Effect of the Fluorescent Dye Rhodamine B Base on Bilayer PDLC Properties

In the set of experiments, different rhodamine B base levels were incorporated into the precursors to explore the influence of different rhodamine B base levels on bilayer PDLC performance. The impact of rhodamine B base content on the electro-optical properties of bilayer PDLC is summarized in Figure 11. Fluorescent dyes can produce fluorescent effects and absorb UV light under UV irradiation, inducing a diminution of light radiation intensity in polymerized monomers. Consequently, the polymerization rate reduces and leads to an expansion of the polymer mesh and LC droplet sizes.

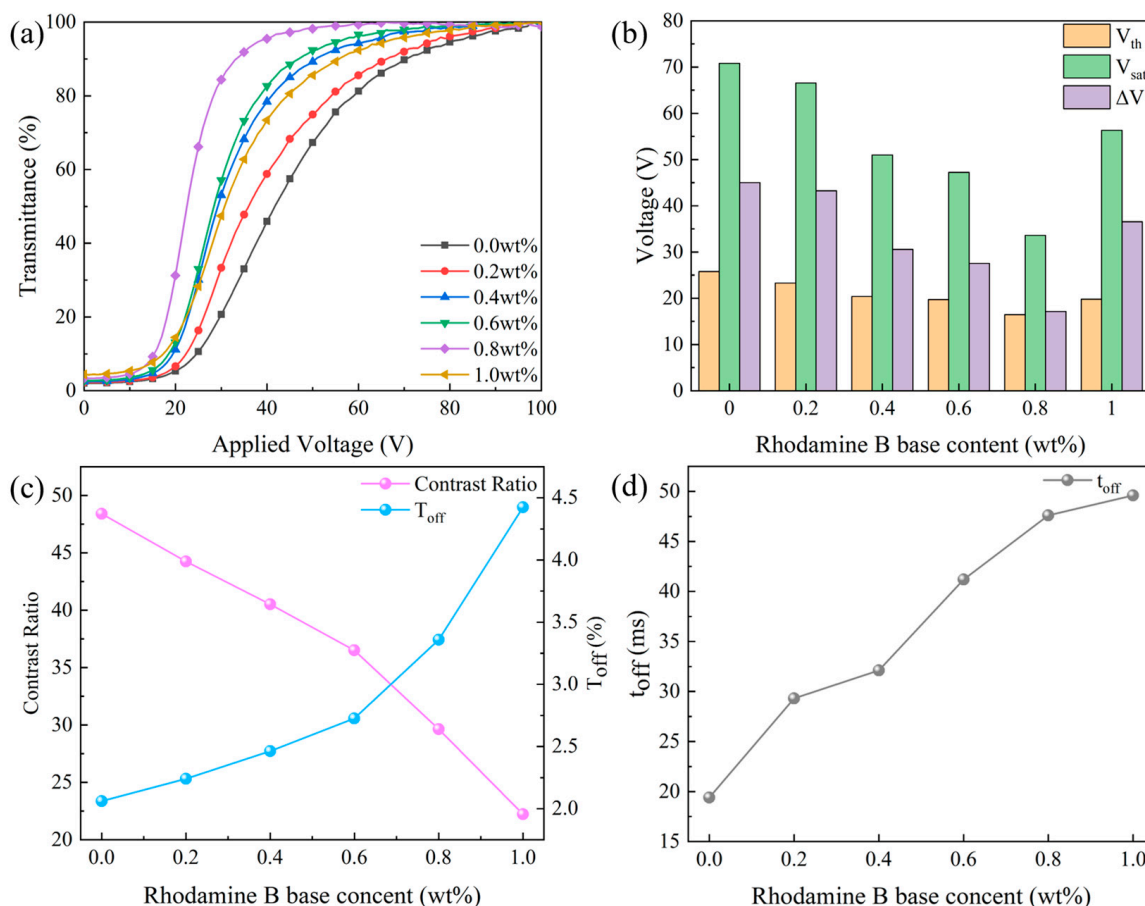


**Figure 11.** The effect of Rhodamine B base content on electro-optical properties. (a) Voltage-transmittance curve; (b) threshold voltage ( $V_{th}$ ), saturation voltage ( $V_{sat}$ ), and  $\Delta V$ ; (c) contrast ratio (CR) and off-state transmittance ( $T_{off}$ ); (d) response time ( $t_{off}$ ).

After the addition of Rhodamine B base proportion from 0 to 0.8 wt%, the transmittance-voltage curve moved to the left and caused a gradual reduction in  $V_{th}$  and  $V_{sat}$  from 25.8 V and 70.8 V to 16.5 V and 33.6 V. With the further increase in rhodamine B base content to 1.0 wt%, the transmittance-voltage curves moved to the right and  $V_{th}$  and  $V_{sat}$  increased to 19.8 V and 56.3 V, as illustrated in Figure 11a,b. The reason for this result is that as the fluorescent dye content increased, the anchoring force on the LC droplets decreased and became easier to drive. However, too much fluorescent dye content led to poor conductivity in the sample, which caused the driving voltage to increase.

Rhodamine B base content also affected the CR of bilayer PDLC, as depicted in Figure 11c. Since  $T_{off}$  gradually decreased with increasing rhodamine B base content, the CR gradually increased. The fluorescent dye increased the refractive index match between the polymer network and LC microdroplets, which increased the  $T_{off}$  of the bilayer PDLC and decreased the CR. In addition, rhodamine B base content affected the

response time of bilayer PDLC, according to Figure 11d. As the anchoring force on LC microdroplets gradually decreased, the time required for their transition from the ordered to the disordered state increased, leading to an increase in  $t_{\text{off}}$ .

The fluorescence emission spectra and visual pictures of bilayer PDLC samples doped with different rhodamine B base percentages are depicted in Figures 12 and 13, respectively. There was a marked upward trend in the fluorescence emission intensity of bilayer PDLC samples as the rhodamine B base content increased. Additionally, there was a series of emission peaks within the metering range, positioned at 590 nm. Compared to no UV irradiation, the samples' orange coloration becomes more pronounced with the increase in rhodamine B base levels, as shown in the physical diagram in Figure 13. One explanation for this is that adding rhodamine B base to PDLC caused a strong fluorescence intensity, which was enhanced by increased fluorescent dye content.

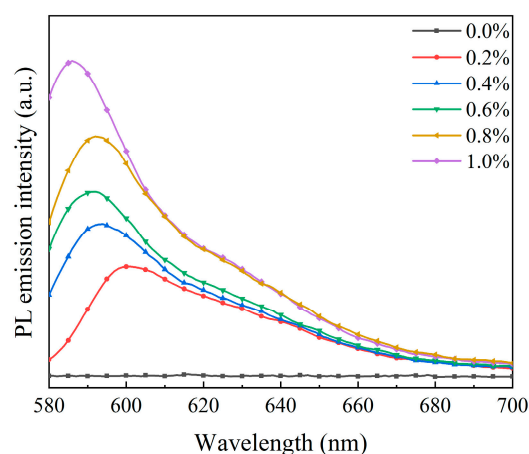


**Figure 12.** Fluorescence emission spectra of bilayer PDLC doped with rhodamine B base.

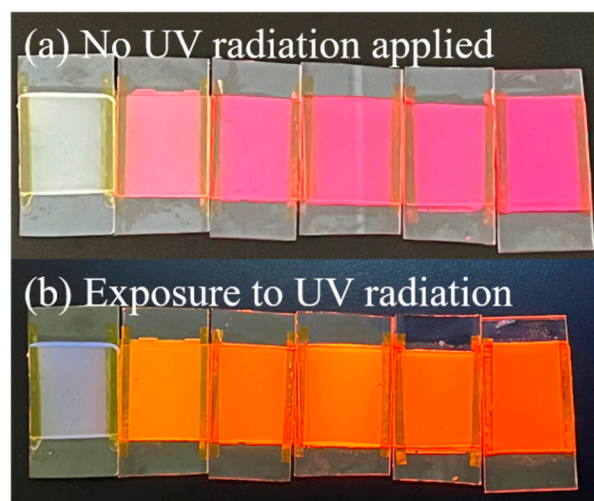


**Figure 13.** Physical image of bilayer PDLC doped with rhodamine B base. (a) No UV radiation applied, (b) Exposure to UV radiation.

### 3.3.2. Progressive Driving Test of Bilayer PDLC Doped with Rhodamine B Base

The physical plots of the transmittance variation of bilayer PDLC doped with rhodamine B base under UV irradiation at different voltages are demonstrated in Figure 14. With the increase of voltage, the transmittance of the bilayer PDLC increases gradually and the pattern at the bottom is clearer, which indicates that the bilayer PDLC sample has favorable progressive driving performance. In addition, due to the fluorescence effect of rhodamine B base, the color of the pattern through the sample changed accordingly.

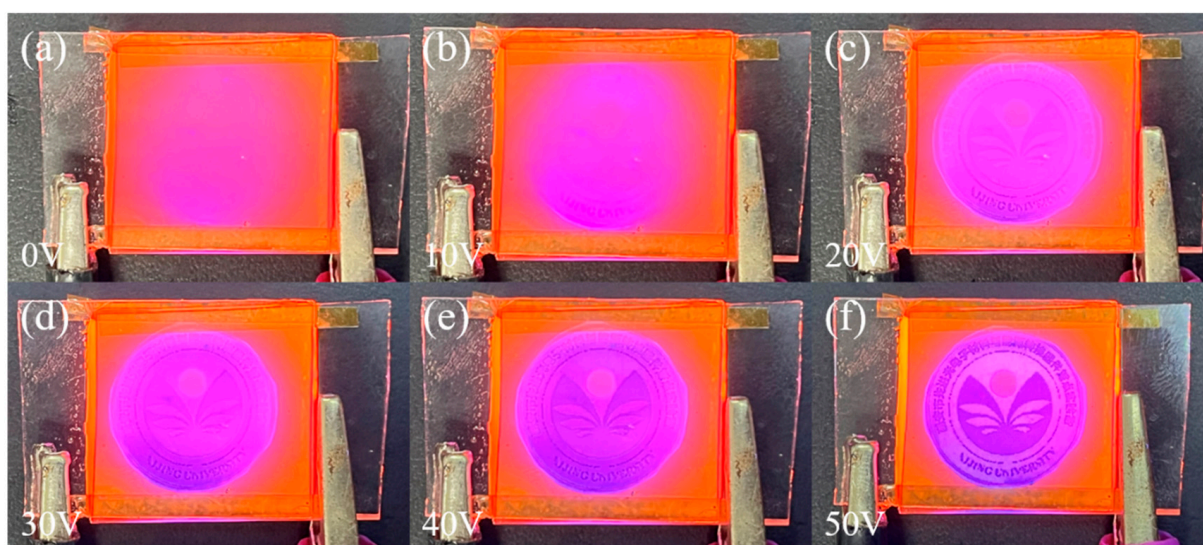


**Figure 14.** Physical plots of transmittance variation of the optimum sample doped with Rhodamine B base at different voltages: (a) 0 V, (b) 10 V, (c) 20 V, (d) 30 V, (e) 40 V, and (f) 50 V, respectively.

### 3.4. High Temperature and Strong UV Light Radiation Tests

The prepared bilayer PDLC samples b2 and c3 were tested for aging resistance in a long-term high temperature (50 °C) and strong UV (830 mW/cm<sup>2</sup>) environment. The test samples were subjected to multiple tests at high temperatures and under UV light to test their electro-optical properties. Specific changes in  $V_{\text{sat}}$  and  $t_{\text{off}}$  are shown in Figure 15, which both increase with aging time. The rate of change in samples doped with rhodamine B base was less than the undoped ones, suggesting that doping with rhodamine B base helps PDLC performance under extreme conditions and has a better lifetime. The presence of rhodamine B base absorbs UV light and converts it to orange light, thereby reducing the damage caused by UV light to the polymer network and providing endless possibilities for future developments.

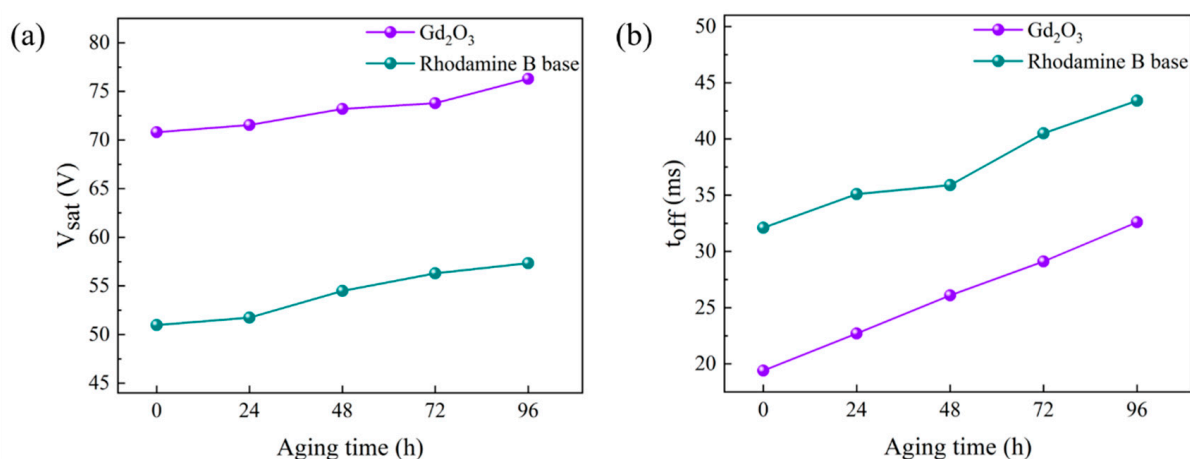


**Figure 15.** Effects of high temperature and strong ultraviolet radiation on (a) saturation voltage ( $V_{\text{sat}}$ ) and (b) response time ( $t_{\text{off}}$ ).

### 3.5. Application of Bilayer PDLC Doped with Rhodamine B Base in Multi-Angle Anti-Counterfeiting

Bilayer PDLC samples doped with rhodamine B base showed orange coloration by fluorescence emission under UV light irradiation. Setting a specific color at a specific location in the pattern can reveal another color when superimposed with the orange color



emitted by the fluorescence of Rhodamine B. Using this feature, PDLC samples doped with rhodamine B base can be applied to the field of anti-counterfeiting. When voltage is applied, the pattern underneath the sample will show a special light after changing the angle of UV irradiation, as shown in Figure 16. When undoped with Rhodamine B, the pattern color is displayed normally. However, when doped with Rhodamine B, special colors develop at specific locations in the pattern. Using UV light to illuminate the sample at different angles will also have different color effects.

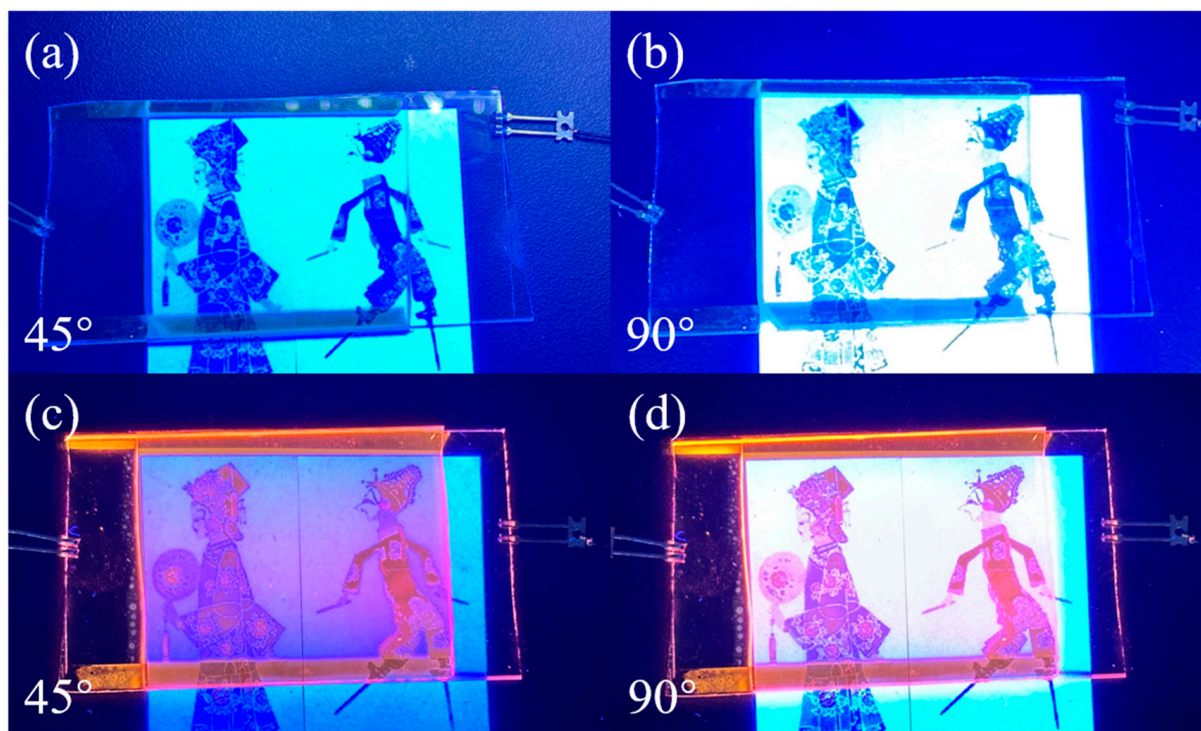


**Figure 16.** Application of bilayer PDLC in anti-counterfeiting. (a) Undoped rhodamine B base and UV 45° oblique light; (b) undoped rhodamine B base and UV 90° direct light; (c) doped rhodamine B base and UV 45° oblique light; (d) doped rhodamine B base and UV 90° direct light.

#### 4. Conclusions

In conclusion, many problems in conventional PDLC devices, such as difficulty accessing the intermediate state between the on-state and the off-state under low-voltage conditions, can be solved by introducing  $\text{Gd}_2\text{O}_3$  nanoparticles and rhodamine B base. According to our experimental results, the polymer network was affected by the ratio of LC/polymerizable monomer, which led to changes in electro-optical properties. In addition, the binding of  $\text{Gd}_2\text{O}_3$  to LC microdroplets and the fluorescence emission from rhodamine B base also affected the polymer mesh, thus conferring excellent electro-optical properties on bilayer PDLCs. Compared to the original samples, samples obtained with  $\text{Gd}_2\text{O}_3$  and rhodamine B base at the optimal content had superior electro-optical properties, with  $V_{\text{th}}$  and  $V_{\text{sat}}$  reduced by about 30% and 35%, respectively. The multi-angle anti-counterfeiting function can also be practiced by the doping of rhodamine B base, leading to innovative application areas for PDLC. Doping with  $\text{Gd}_2\text{O}_3$  nanoparticles and fluorescent dye rhodamine B base not only improved electro-optical properties but also the functionalization of PDLC films. This study provides promising new ideas for preparing functional PDLC devices.

**Author Contributions:** Conceptualization, Y.W., X.L., D.W. and L.W.; data curation, Y.W.; formal analysis, Y.W. and Z.G.; funding acquisition, Y.Z.; investigation, Y.W. and H.G.; methodology, Y.W. and Y.L.; project administration, Y.Z.; resources, Y.Z., Z.G., D.W. and L.W.; software, Y.W., X.L. and H.G.; validation, Y.W. and X.L.; visualization, Y.W.; writing—original draft, Y.W.; writing—review and editing, Y.W., D.W. and Y.L. All authors have read and agreed to the published version of the manuscript.

**Funding:** This work was supported by the Natural Science Basic Research Plan in Shaanxi Province of China (Program No. 2024JC-YBMS-342), the Natural Science Foundation of Shaanxi Provincial Department of Education (Program No. 22JP100), Science and technology plan project of Xi'an (No. 22GXFW0150), National Natural Science Foundation of China (No. 51971182), Xi'an Science and Technology Plan Project of Shaanxi Province (No. 23LLRH0008), and the Youth Innovation Team of Shaanxi Universities.

**Institutional Review Board Statement:** Not applicable.

**Informed Consent Statement:** Not applicable.

**Data Availability Statement:** The data presented in this study are available in article.

**Conflicts of Interest:** The authors declare no conflict of interest.

## References

1. Zhang, H.M.; Miao, Z.C.; Shen, W.B. Development of polymer-dispersed liquid crystals: From mode innovation to applications. *Compos. Part A Appl. Sci. Manuf.* **2022**, *163*, 107234. [[CrossRef](#)]
2. Hemaida, A.; Ghosh, A.; Sundaram, S.; Mallick, T.K. Simulation study for a switchable adaptive polymer dispersed liquid crystal smart window for two climate zones (Riyadh and London). *Energ. Build.* **2021**, *251*, 111381. [[CrossRef](#)]
3. Li, K.; Wang, J.W.; Cai, W.F.; He, H.L.; Cen, M.J.; Liu, J.X.; Luo, D.; Mu, Q.Q.; Gérard, D.; Liu, Y.J. Electrically switchable, polarization-sensitive encryption based on aluminum nanoaperture arrays integrated with polymer-dispersed liquid crystals. *Nano Lett.* **2021**, *21*, 7183–7190. [[CrossRef](#)] [[PubMed](#)]
4. Kumar, S.; Kang, D.; Nguyen, V.H.; Nasir, N.; Hong, H.; Kim, M.; Nguyen, D.C.; Lee, Y.J.; Lee, N.; Seo, Y. Application of titanium-carbide MXene-based transparent conducting electrodes in flexible smart windows. *ACS Appl. Mater. Interfaces* **2021**, *13*, 40976–40985. [[CrossRef](#)] [[PubMed](#)]
5. Kamal, W.; Li, M.M.; Lin, J.D.; Parry, E.; Jin, Y.H.; Elston, S.J.; Castrejón-Pita, A.A.; Morris, S.M. Spatially patterned polymer dispersed liquid crystals for image-integrated smart windows. *Adv. Opt. Mater.* **2022**, *10*, 2101748. [[CrossRef](#)]
6. Iluyemi, D.C.; Nundy, S.; Shaik, S.; Tahir, A.; Ghosh, A. Building energy analysis using EC and PDLC based smart switchable window in Oman. *Sol. Energy* **2022**, *237*, 301–312. [[CrossRef](#)]
7. Gong, S.; Cao, Y.; Fang, X.; Wang, Y.F.; Liu, Q.Z.; Gui, H.; Shen, C.F.; Cao, X.; Kim, E.S.; Zhou, C.W. Carbon nanotube macroelectronics for active matrix polymer-dispersed liquid crystal displays. *ACS Nano* **2016**, *10*, 10068–10074.
8. Manabe, H.; Date, M.; Takada, H.; Inamura, H. Techniques to reduce driving energy of 1-pixel displays. *IEEE Trans. Ind. Appl.* **2016**, *52*, 2638–2647. [[CrossRef](#)]
9. Zhang, C.; Wang, H.L.; Guan, S.; Guo, Z.H.; Zheng, X.X.; Fan, Y.J.; Wang, Y.; Qu, T.; Zhao, Y.B.; Chen, A.H.; et al. Self-powered optical switch based on triboelectrification-triggered liquid crystal alignment for wireless sensing. *Adv. Funct. Mater.* **2019**, *29*, 1808633. [[CrossRef](#)]
10. Van, M.C.W.; Janssen, R.H.C.; Broer, D.J.; Wilderbeek, H.T.A.; Bastiaansen, C.W.M. Polymer-filled nematics: A new class of light-scattering materials for electro-optical switches. *Adv. Mater.* **2000**, *12*, 753–757.
11. Baars, M.W.P.L.; Van, M.C.W.; Bastiaansen, C.W.M.; Broer, D.J.; Söntjens, S.H.M.; Meijer, E.W. A scattering electro-optical switch based on dendrimers dispersed in liquid crystals. *Adv. Mater.* **2000**, *12*, 715–719. [[CrossRef](#)]
12. Ghosh, A. Diffuse transmission dominant smart and advanced windows for less energy-hungry building: A review. *J. Build. Eng.* **2023**, *64*, 105604. [[CrossRef](#)]
13. Mesloub, A.; Ghosh, A.; Kolsi, L.; Alshenaifi, M. Polymer-dispersed liquid crystal (PDLC) smart switchable windows for less-energy hungry buildings and visual comfort in hot desert climate. *J. Build. Eng.* **2022**, *59*, 105101. [[CrossRef](#)]
14. Ghosh, A. Investigation of vacuum-integrated switchable polymer dispersed liquid crystal glazing for smart window application for less energy-hungry building. *Energy* **2023**, *265*, 126396. [[CrossRef](#)]
15. Ma, M.F.; Zhao, Y.Z.; Gao, H.; Wang, D.; Miao, Z.C.; Cao, H.; Yang, Z.; He, W.L. Role of semiconductor nanoparticles on electro-optical performance of PDLC devices. *Liq. Cryst.* **2022**, *49*, 2058–2068. [[CrossRef](#)]
16. Seo, J.; Song, M.; Jeong, J.; Nam, S.; Heo, I.; Park, S.Y.; Kang, I.K.; Lee, J.H.; Kim, H.; Kim, Y. Broadband pH-sensing organic transistors with polymeric sensing layers featuring liquid crystal microdomains encapsulated by di-block copolymer chains. *ACS Appl. Mater. Interfaces* **2016**, *8*, 23862–23867. [[CrossRef](#)] [[PubMed](#)]

17. Khelifi, S.; Bignon, J.; Amela-Cortes, M.; Dumait, N.; Loas, G.; Cordier, S.; Molard, Y. Switchable two-dimensional waveguiding abilities of luminescent hybrid nanocomposites for active solar concentrators. *ACS Appl. Mater. Interfaces* **2020**, *12*, 14400–14407. [\[CrossRef\]](#)
18. Ailincal, D.; Marin, L. Eco-friendly PDLC composites based on chitosan and cholesteryl acetate. *J. Mol. Liq.* **2021**, *321*, 114466. [\[CrossRef\]](#)
19. Li, Y.; Gong, C.D.; Li, C.G.; Ruan, K.P.; Liu, C.; Liu, H.; Gu, J.W. Liquid crystalline texture and hydrogen bond on the thermal conductivities of intrinsic thermal conductive polymer films. *J. Mater. Sci. Technol.* **2021**, *82*, 250–256. [\[CrossRef\]](#)
20. Deng, Y.; Yang, Y.H.; Xiao, Y.H.; Xie, H.L.; Lan, R.C.; Zhang, L.Y.; Yang, H. Ultrafast switchable passive radiative cooling smart windows with synergistic optical modulation. *Adv. Funct. Mater.* **2023**, *33*, 2301319. [\[CrossRef\]](#)
21. Cheng, Z.X.; Wang, T.J.; Li, X.; Zhang, Y.H.; Yu, H.F. NIR-Vis-UV light-responsive actuator films of polymer-dispersed liquid crystal/graphene oxide nanocomposites. *ACS Appl. Mater. Interfaces* **2015**, *7*, 27494–27501. [\[CrossRef\]](#) [\[PubMed\]](#)
22. Zhang, P.; Tong, X.R.; Gao, Y.; Qian, Z.Y.; Ren, R.R.; Bian, C.C.; Wang, J.H.; Cai, G.F. A sensing and stretchable polymer-dispersed liquid crystal device based on spiderweb-inspired silver nanowires-micromesh transparent electrode. *Adv. Funct. Mater.* **2023**, *33*, 2303270. [\[CrossRef\]](#)
23. Shivaraja, S.J.; Gupta, R.K.; Manjuladevi, V. Faster switching polymer dispersed liquid crystal devices incorporated with functionalized SWCNTs. *J. Mol. Liq.* **2022**, *354*, 118905. [\[CrossRef\]](#)
24. Nasir, N.; Kumar, S.; Kim, M.; Nguyen, V.H.; Suleman, M.; Park, H.M.; Lee, S.; Kang, D.; Seo, Y. Effect of the photoinitiator concentration on the electro-optical properties of thiol-acrylate-based PDLC smart windows. *ACS Appl. Energy Mater.* **2022**, *5*, 6986–6995. [\[CrossRef\]](#)
25. Shi, Z.H.; He, Z.M.; Li, C.S.; Miao, Z.C.; Wang, D.; Luan, Y.; Li, Y.Z.; Zhao, Y.Z. The role of nanomesh fibres loaded with fluorescent materials on the electro-optical performance of PDLC devices. *Liq. Cryst.* **2022**, *49*, 2037–2050. [\[CrossRef\]](#)
26. Kim, E.; Liu, Y.; Hong, S.J.; Han, J.I. Effect of SiO<sub>2</sub> nanoparticle doping on electro-optical properties of polymer dispersed liquid crystal lens for smart electronic glasses. *Nano Converg.* **2015**, *2*, 5. [\[CrossRef\]](#)
27. Katariya-Jain, A.; Mhatre, M.M.; Dierking, I.; Deshmukh, R.R. Enhanced thermo-electro-optical and dielectric properties of carbon nanoparticle-doped polymer dispersed liquid crystal based switchable windows. *J. Mol. Liq.* **2024**, *393*, 123575. [\[CrossRef\]](#)
28. Zhang, Z.G.; Song, Y.Z.; Zhang, B.; Wang, L.; He, X.M. Metallized plastic foils: A Promising solution for high-energy lithium-ion battery current collectors. *Adv. Energy Mater.* **2023**, *13*, 2370146. [\[CrossRef\]](#)
29. Peng, S.J.; Du, X.F.; Liang, Z.S.; Ma, M.B.; Guo, Y.; Xiong, L.L. Multilayer polymer nanocomposites based on interface engineering for high-performance capacitors. *J. Energy Storage* **2023**, *60*, 106636. [\[CrossRef\]](#)
30. Khoi, T.M.; Tran, N.A.T.; Jung, H.B.; Huynh, V.P.; Kim, Y.; Hong, J.; Yoo, C.Y.; Kang, H.S.; Cho, Y. Selective and continuous ion recovery using flow electrode capacitive deionization with polymer multilayers functionalized ion exchange membrane. *Desalination* **2023**, *558*, 116626. [\[CrossRef\]](#)
31. Culebras, M.; Byun, Y.Y.; Jang, J.; Serafin, A.; Collins, M.N.; Park, Y.T.; Cho, C. Nanostructured PEDOT-based multilayer thin films with high thermoelectric performances. *Appl. Surf. Sci.* **2023**, *615*, 156432. [\[CrossRef\]](#)
32. Park, H.; Mong, A.L.; Kim, D. Single and multilayer composite electrolytes for enhanced Li-ion conductivity with restricted polysulfide diffusion for lithium-sulfur battery. *Mater. Today Energy* **2023**, *33*, 101274. [\[CrossRef\]](#)
33. Eslami, H.; Mekonnen, T.H. Flexible and green multilayer paper coating for barrier enhancement of paper packaging. *Sustain. Mater. Technol.* **2023**, *37*, e00694. [\[CrossRef\]](#)
34. Ogura, H.; Kawasaki, S.; Liu, Z.; Endo, T.; Maruyama, M.; Gao, Y.L.; Nakanishi, Y.; Lim, H.E.; Yanagi, K.; Irisawa, T.; et al. Multilayer in-plane heterostructures based on transition metal dichalcogenides for advanced electronics. *ACS Nano* **2023**, *17*, 6545–6554. [\[CrossRef\]](#)

**Disclaimer/Publisher's Note:** The statements, opinions and data contained in all publications are solely those of the individual author(s) and contributor(s) and not of MDPI and/or the editor(s). MDPI and/or the editor(s) disclaim responsibility for any injury to people or property resulting from any ideas, methods, instructions or products referred to in the content.